Composition, structure, and stability of the rutile TiO$_2$(110) surface: Oxygen depletion, hydroxylation, hydrogen migration, and water adsorption

Piotr M. Kowalski,[1] Bernd Meyer,[1,2] and Dominik Marx[1]

[1]*Lehrstuhl für Theoretische Chemie, Ruhr-Universität Bochum, 44780 Bochum, Germany*
[2]*Interdisziplinäres Zentrum für Molekulare Materialien (ICMM) and Computer-Chemie-Centrum (CCC),
Universität Erlangen-Nürnberg, 91052 Erlangen, Germany*

A comprehensive phase diagram of lowest-energy structures and compositions of the rutile TiO$_2$(110) surface in equilibrium with a surrounding gas phase at finite temperatures and pressures has been determined using density-functional theory in combination with a thermodynamic formalism. The exchange of oxygen, hydrogen, and water molecules with the gas phase is considered. Particular attention is given to the convergence of all calculations with respect to lateral system size and slab thickness. In addition, the reliability of semilocal density functionals in describing the energetics of the reduced surfaces is critically evaluated. For ambient conditions the surface is found to be fully covered by molecularly adsorbed water. At low coverages, in the limit of single isolated water molecules, molecular and dissociative adsorption modes become energetically degenerate. Oxygen vacancies form in strongly reducing, oxygen-poor environments. However, already at slightly more moderate conditions it is shown that removing full TiO$_2$ units from the surface is thermodynamically preferred. In agreement with recent experimental observations it is furthermore confirmed that even under extremely hydrogen-rich environments the surface cannot be fully hydroxylated, but only a maximum coverage with hydrogen of about 0.6–0.7 monolayer can be reached. Finally, calculations of migration paths strongly suggest that hydrogen prefers diffusing into the bulk over desorbing from the surface into the gas phase.

I. INTRODUCTION

Over the past years, the (110) surface of TiO$_2$ in the rutile structure has become one of the most popular model systems for fundamental surface science studies of transition-metal oxides.[1] It is the thermodynamically most stable crystal face of TiO$_2$ and therefore represents the dominating facet of rutile crystallites.[2] Stoichiometric single-crystal (1×1) surfaces may be easily prepared, and most experimental surface science techniques can be applied without difficulties.[1] The interest in TiO$_2$(110) surfaces is furthermore driven by many technological applications of TiO$_2$, ranging from pigments, coatings, electronic devices, implants, gas sensors, and photochemical reactions to catalysis. In all of them, the surface properties of TiO$_2$ play a crucial role.[1]

One of the most important properties of TiO$_2$ is that it can be easily reduced. The reducibility is essential for many applications of TiO$_2$ in heterogeneous catalysis. Oxide-supported metal-based catalysts with TiO$_2$ as part of the support often show a so-called strong metal-support interaction (SMSI).[3] Here, the catalytic properties of the supported metal clusters are profoundly modified by an incorporation of partially reduced TiO$_x$ into the boundary areas of the metal particles.[4] In many cases, the TiO$_x$-decorated metal particles exhibit a much higher catalytic activity for hydrogenation reactions than the pure metal itself.[5]

One way to reduce the TiO$_2$(110) surface is to remove surface O atoms. By this process, formally two neighboring Ti^{4+} ions of a vacancy change to a Ti^{3+} oxidation state. In ultrahigh vacuum (UHV) experiments O vacancies are easily created either by electron bombardment, by sputtering, or simply by annealing. The presence of O vacancies strongly increases the reactivity of the surface. Among the many in-vestigated processes, probably the best studied surface reaction is the dissociation of water, which has been shown to occur at O vacancies,[6–10] whereas on the stoichiometric, well-annealed parts of the surface the water molecules stay mostly intact.[11–13] There is, however, a limit to what extent the surface can be reduced. Oxygen vacancy concentrations are typically on the order of several percent,[12,14] but it is not possible to remove all surface O atoms, in contrast to, for example, the rutile SnO$_2$(101) surface.[15,16]

Alternatively, the TiO$_2$(110) surface can be reduced by hydroxylation of the surface O atoms via adsorption of hydrogen. While on unreducible oxides, such as MgO, a heterolytic dissociative adsorption of H$_2$ with H$^+$ adsorbing on O^{2-} and H$^-$ on the metal cations is preferred, it is more favorable for reducible oxides, such as TiO$_2$, to form only OH$^-$ groups. In the latter case the excess electrons are transferred to the cations, thus reducing Ti^{4+} to Ti^{3+}.

The interaction of hydrogen with TiO$_2$(110), however, has been much less intensively investigated by surface science studies than the reduction by O depletion. This is rather surprising in view of the importance of TiO$_2$ as catalyst component for hydrogenation reactions and the prospective application of TiO$_2$ as photocatalyst for the decomposition of water. It has been shown that molecular hydrogen does not interact strongly with TiO$_2$(110),[17,18] while atomic hydrogen readily sticks to the surface O atoms.[18–21] No Ti-H vibrations could be detected with high-resolution electron-energy-loss spectroscopy (HREELS).[21] Interestingly, also the reducibility of TiO$_2$(110) with hydrogen is limited. Recent scanning-tunneling microscopy (STM) measurements[21] revealed that even after very high exposures to atomic hydrogen, the surface cannot be saturated. Only a maximum coverage of about 0.7 monolayers (ML) could be achieved. The scattering of

thermal energy He atoms (HAS) showed that the hydroxyl groups do not form an ordered overlayer.[18] Performing a thermal-desorption spectroscopy (TDS) experiment by monitoring the He atom reflectivity of the surface while increasing the temperature (He-TDS), two distinct changes in the reflectivity at 388 and 626 K were observed, which indicate structural rearrangements of the surface.[18] These rearrangements must involve the loss of the hydrogen atoms since afterward the surface was H free, as seen by HAS and HREELS. However, in conventional TDS there is no desorption of H$_2$, and only a very small amount of H$_2$O was detected,[21] even after heating the surface up to 650 K. This led to the conclusion that the H atoms diffuse into the bulk rather than desorb from the surface.[21]

As for experiment, theoretical studies of reduced TiO$_2$(110) have mainly focused on O-deficient surfaces. While the properties of O vacancies on TiO$_2$(110) have been investigated extensively[22–34] (see Ref. [35] for a recent review), we are aware of only two recent studies addressing specifically the adsorption of hydrogen.[21,36] The determination of binding energies, adsorption sites, and some reaction barriers, however, was restricted in both cases to slabs with a (1×1) periodicity, thus assuming H coverages of one and more H atoms per surface unit cell.

Finally, next to the formation of O vacancies and the hydroxylation of the surface by hydrogen adsorption, the interaction with water also has to be taken into account. The adsorption of water, either molecular or dissociative, does not lead to a reduction of the surface. But since water is always present, even in well-controlled UHV experiments, one has to account for residual hydroxyl groups which affect other adsorption and reaction processes.[1] Water adsorption on TiO$_2$(110) has been investigated extensively both experimentally and theoretically. Among the experimental studies the common view is that at all coverages water adsorbs molecularly on the ideal terraces of the TiO$_2$(110) surface and only dissociates at defects.[1,11–13] However, it should be noted that in all these experiments always a small amount of dissociated water was present as seen by x-ray photoemission spectroscopy (XPS) and HREELS and indicated by a high-temperature tail in TDS. These signatures were naturally attributed to water molecules dissociated at O vacancies, but it would be difficult to distinguish them from a situation in which water initially would adsorb dissociatively at very low coverages and molecularly afterward as suggested by some early studies.[11,37] In contrast to the consensus among the experimental studies the results from theoretical calculations are very contradictory. Early investigations predicted water dissociation at all coverages, in complete disagreement with experiment. Only in some more recent calculations partial dissociated or molecular structures of water were found to be lower in energy. Overall, the theoretical studies are almost evenly divided whether molecular, dissociative, or partial dissociative adsorption of water (strongly depending on the coverage) is predicted as the energetically most stable state.[38–47]

The aim of the present paper is to explore the competition between the reduction of the TiO$_2$(110) surface via O vacancy formation or hydrogen adsorption and the nonreductive interaction of the surface with water in a comprehensive

and systematic way. For a series of surface models with different O defect configurations and for a wide range of both hydrogen and water coverages, we determine the total energies and the fully relaxed atomic structures using first-principles density-functional theory (DFT). In order to extend the zero-temperature and zero-pressure DFT results to relevant environmental situations, such as UHV or reaction conditions in heterogenous catalysis, and to identify the thermodynamically most stable surface structures and compositions depending on the experimental conditions, we assume that the surfaces are in thermodynamic equilibrium with a surrounding gas phase at a given temperature T and finite partial pressures p. To account for the exchange of oxygen and hydrogen between the surface and the gas phase, appropriate chemical potentials $\mu_O(T,p)$ and $\mu_H(T,p)$ are introduced.[48–51] By minimizing the surface Gibbs free energy as function of the chemical potentials, surface phase diagrams of the most stable surface structure and composition are constructed depending on both temperature and partial pressures.[48–51]

Within this context the main focus of the present study will be the hydroxylated surface. In addition to the thermodynamic considerations, we investigate the kinetic behavior of hydrogen atoms and water molecules on the TiO$_2$(110) surface. Energy barriers for various surface processes related to the migration and desorption of hydrogen and to the dissociation of water are calculated. Our results support the recently proposed suggestion that hydrogen atoms, instead of being desorbed from the surface at higher temperatures, migrate into the bulk. In addition, we find a rather small barrier for water dissociation. However, in contrast to some previous studies, our results indicate that the molecular adsorption of water is preferred over dissociation in the monolayer coverage limit.

II. COMPUTATIONAL APPROACH

The DFT calculations for the different TiO$_2$(110) surface structures, as well as the bulk and molecular reference energies, have been carried out using the Car-Parrinello Molecular Dynamics (CPMD) code.[52,53] The gradient-corrected Perdew-Burke-Ernzerhof functional[54] PBE was used to describe the exchange and correlation effects. Vanderbilt ultrasoft pseudopotentials[55] were employed together with a plane-wave basis set to represent the Kohn-Sham orbitals. A plane-wave cutoff energy of 25 Ry was sufficient to get well-converged results for structures and energetics. In particular, increasing the cutoff to 30 Ry changed the adsorption energies for water molecules by less than 0.02 eV. The Ti pseudopotential was constructed from an ionic $3d^14s^2$ configuration, and the $3s$ and $3p$ semicore electrons were treated as full valence states. Since very large supercells were used (see below), the k-point sampling was restricted to the Γ point. Spin polarization was included for all systems with an odd number of electrons and for all calculations with oxygen vacancies. All configurations were relaxed by minimizing the atomic forces. Convergence was assumed when the maximum component of the residual forces on the ions was less than 0.01 eV/Å.

With this computational setup we find for the optimized TiO_2 bulk lattice parameters values of $a = 4.649$ Å, $c = 2.966$ Å, and $u = 0.305$, which compare very well to previous generalized gradient approximation (GGA) calculations[23,30,31,39,44,56,57] and to experiment ($a = 4.594$ Å, $c = 2.959$ Å, and $u = 0.305$; see Ref. [58]).

For the calculation of the energetics of O vacancy formation as well as hydrogen and water adsorption, the total energies of the isolated O_2, H_2, and H_2O molecules are needed. While H_2 and H_2O are reasonably well described within PBE-DFT, it is a well-known deficiency of all local and semilocal functionals (such as PBE) that they strongly overbind the O_2 molecule.[26,28,29,35,50,59] In our setup we find an O_2 binding energy of 5.87 eV, which is about 0.4 eV lower than the fully converged PBE value of 6.24 eV,[54,60] which is in turn about 1 eV larger than the experimental value[61] of 5.26 eV [with zero-point vibration energy (ZPE) removed in the harmonic approximation].

In order to circumvent errors introduced by a poor description of the O_2 molecule, we do not employ the total energy of the O_2 molecule from the DFT calculation as reference, but deduce it via a thermodynamic cycle from the total energies of the H_2 and H_2O molecules together with the experimental value of 2.51 eV (Ref. [61]) for the formation energy of water from H_2 and O_2 (also taking into account the corrections due to zero-point vibrations). With this reference energy for the gas phase O_2 molecule, we obtain a formation energy of bulk TiO_2 from metallic bulk Ti and O_2 of 9.60 eV, which is in excellent agreement with the experimental formation enthalpy of 9.73 eV.[61]

The second problem we have to address is how reliable can we expect the DFT calculations to be when describing the reduced state of an insulator or semiconductor.[62] It is a well-known shortcoming of local density approximation (LDA) and all commonly used GGA functionals that band gaps are substantially underestimated due to the insufficient cancellation of the self-interaction energy. With our setup we find a band gap for bulk TiO_2 of 1.86 eV, which is in very good agreement with previous DFT calculations,[22–24,56,63] but is much smaller than the experimental value of 3.03 eV,[64] as expected. Upon reduction, defect states are created, which typically appear in the band-gap region. In DFT calculations, however, due to the underestimation of the band gap, they might be placed erroneously into the conduction band. In such a case, a delocalized conduction-band state and not the localized defect state would be occupied with electrons. In particular, this is partially true for O vacancies on $TiO_2(110)$. Experiment indicates that the O vacancies are responsible for a defect state about 0.7–0.9 eV below the conduction-band edge.[37,65,66] A careful survey of the available literature data[35] showed, however, that in well-converged GGA-DFT calculations this defect level is pinned at the bottom of the conduction band, giving rise to a defect state which is too delocalized.

The problem of both the band gap and the position of the defect levels could be cured to a large extent by employing hybrid density functionals.[25,32,35,67] Unfortunately, for extensive studies using large supercells as required for the present purpose, they are computationally still very demanding even if localized basis sets are used. On the other hand, the review
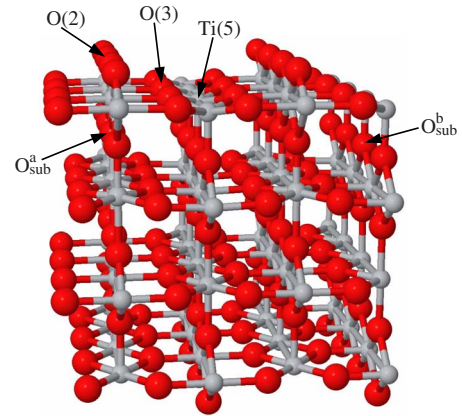

FIG. 1. (Color online) Atomic structure of the stoichiometric rutile $TiO_2(110)$ surface. Oxygen atoms are shown in red; Ti atoms are shown in gray. The two- and threefold-coordinated O sites and the fivefold-coordinated Ti sites are labeled as O(2), O(3), and Ti(5), respectively.

in Ref. [35] surprisingly reveals that despite the problem of the correct position of the defect level, GGA-DFT calculations give quite good results for the *energetics* of the defect formation. While the best estimate for the O vacancy formation energy using a cluster model and the B3LYP hybrid functional is 2.7 eV (which relies on extrapolations to account for the finite cluster size and the limited atomic relaxation in this calculation, thus adding some uncertainty to this value),[35] the converged DFT result (using the generalized gradient functional PW91, PBE, or RPBE) is 3.0 eV.[35] It is in particular noticeable that despite the underestimation of the band gap and the too strong delocalization of the defect state, the DFT calculations *overestimate* the vacancy formation energy and thus underestimate the reducibility of TiO_2.

In recent experiments it was shown that the dissociative adsorption of water at O vacancies (thereby forming two neighboring OH groups on the surface) does not change significantly the O vacancy–induced defect state in the band gap (which was seen 0.9 eV below the conduction-band edge).[68] Also for this hydrogen-reduced state of the $TiO_2(110)$ surface (which can be viewed as adsorbing an H_2 molecule on the defect-free surface instead of dissociating a water molecules at an O vacancy), Di Valentin *et al.*[67] found that the defect state is not separated from the conduction band in GGA-DFT calculations. Nevertheless, despite this problem of accurately describing the electronic structure, we will argue in the present paper that the GGA-DFT calculations still give quite reliable results for the *energetics* of reduced surfaces via hydroxylation, similar to what we have seen for the surface reduction via O vacancy formation. In particular in the regime of higher H coverages, when the defect states start to interact and a defect band is formed which will gradually hybridize with the conduction band, the DFT calculations will be less and less hampered by the band-gap problem.

Figure [1] shows the atomic structure of the stoichiometric $TiO_2(110)$ surface. In our calculations all surface structures were modeled by periodically repeated slabs. Slabs for the stoichiometric (110) surface are built by a stacking sequence
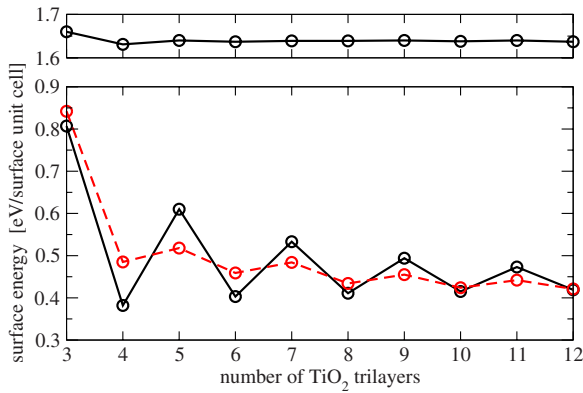
FIG. 2. (Color online) Convergence of the unrelaxed (upper panel) and relaxed (lower panel) $TiO_2(110)$ surface energies with slab thickness; note the different energy scales. The solid black line in the lower panel represents the result from fully relaxed slabs. The calculation with the atoms in the bottom two trilayers fixed at the bulk positions is shown by the red dashed line.

FIG. 3. (Color online) Convergence of the hydrogen adsorption energy E_{ad}^H with slab thickness at full monolayer coverage. The atoms in the bottom two trilayers were fixed at the bulk positions. The solid black and the dashed red lines distinguish calculations without and with saturation of the broken surface bonds at the bottom of the slabs with pseudohydrogen atoms with nucleus charges of $+4/3$ and $+2/3$, respectively.

of trilayers with a composition of O-Ti_2O_2-O. In the bulk, the Ti and O ions are sixfold and threefold coordinated, respectively. At the surface this coordination is reduced and the characteristic feature of the (110) surface is the presence of rows of twofold-coordinated bridging O ions parallel to fivefold-coordinated Ti atom along the [001] direction. Using formal ionic charges of $+4$ and -2 for the Ti and O ions, respectively, the stoichiometric (110) surface would be charge neutral. From a more covalent point of view, the (110) surface, as shown in Fig. 1, is created by a cleavage of the crystal in which the minimum possible number of bonds has been broken.

The surface energy for the unrelaxed slabs converges very fast with slab thickness as shown in Fig. 2. After a full relaxation, however, the surface energy shows strong odd-even oscillations with the number of trilayers in the slab (see Fig. 2). A very large number of trilayers would be needed to get well-converged results. These oscillations have been noted previously[2,29,56,57,69,70] and are also present in plots of vacancy formation[28,30,69] and water adsorption energies.[44–47] The odd-even oscillations arise from the different symmetry of the slabs which leads to a significant change in the hybridization of the O $2p$ and Ti $3d$ states in the direction of the surface normal.[56] In slabs with an even number of trilayers the O-Ti hybridization causes a modulation of the coupling between the trilayers in such a way that a sequence of pairs of trilayers is formed in which the coupling of the trilayers within the pair is stronger than the interaction between pairs.[56] For slabs with an odd number of trilayers, in contrast, the atomic relaxations, which are associated with this pair formation, are suppressed by the central Ti_2O_2 mirror plane and the O-Ti hybrid orbitals become more delocalized over the whole slab.[56] The surface energy of the slabs with an odd number is higher and the convergence to the limit of infinite slab thickness is slower than when using an even number of trilayers. The odd-even oscillations can be largely reduced if not the full slab is allowed to relax. In Fig. 2 the surface energy is shown for a calculation in which the atoms in the bottom two trilayers were held fixed at their bulk
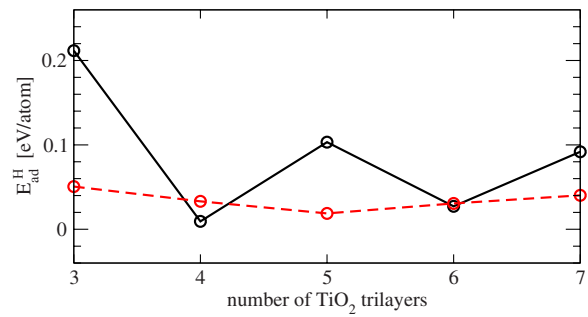
positions. Using this setup, quite well-converged results are already obtained with only four trilayers.

Based on this observation Thompson and Lewis[57] proposed to use such a slab setup of four trilayers with the bottom two layers fixed for any large-scale calculation. However, the surface properties of a stoichiometric slab might be less influenced by the slab thickness than when it comes to reduced surface structures. States above the valence band (either defect states in the band gap or states from the lower edge of the conduction band) are more delocalized than the valence states and might be more sensitive to the truncation at the bottom of the slab. For example, Leconte *et al.*[36] reported that for fully hydroxylated slabs with a thickness of two trilayers, only 63% of the spin density is localized at the hydroxylated top surface layer, but 37% is at the bottom of the slab. The fully hydroxylated surface is the highest reduced state which we will consider in our calculations (though, as we will show in Sec. III B, this configuration is thermodynamically not stable). Even after fixing the atomic positions of the bottom two trilayers to the bulk positions, the hydrogen adsorption energy at monolayer coverage still shows a slow convergence and noticeable oscillations with slab thickness, as can be seen in Fig. 3.

Though TiO_2 is a strong ionic insulator, the chemical bond has significant covalent contributions. It is therefore worth thinking about the TiO_2 surface in terms of broken surface bonds as one would do for covalent semiconductor surfaces.[71] Ti and O have four and six valence electrons, respectively. To fulfill the octet rule, each O atom receives $2/3$ electrons from its three nearest Ti neighbors and Ti contributes $4/6$ electrons to each of its six nearest-neighbor bonds. At the $TiO_2(110)$ surface the fivefold Ti and the twofold bridging O atoms have lost one of their nearest-neighbor atoms. Thus, dangling bonds are created which are occupied with $2/3$ electrons for the fivefold Ti(5) and $4/3$ electrons for the twofold O(2). At the stoichiometric surface the partial occupation of these dangling bonds is removed by autocompensation.[71] Alternatively, we saturate these broken bonds at the bottom of the slab by introducing artificial atoms with nucleus charges of $+4/3$ and $+2/3$ which we place next to the Ti(5) and O(2) atoms, respectively, thus creating a
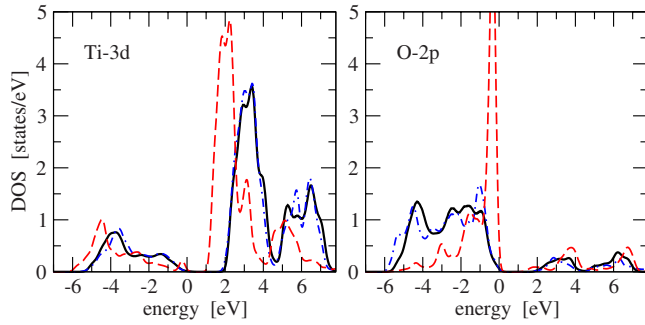
FIG. 4. (Color online) Local densities of states (LDOS) of Ti and O atoms in bulk TiO₂ (black solid lines), of the fivefold- and twofold-coordinated Ti(5) and O(2) surface atoms at the bottom of a four-trilayer TiO₂(110) slab (top two layers relaxed, bottom two layers fixed at bulk positions; red dashed lines), and after saturation of the bottom Ti(5) and O(2) surface atoms with pseudohydrogen atoms (see text; blue dashed-dotted lines). The top of the valence band is at 0 eV.

more bulklike environment for these surface atoms.[72] The distance between the pseudohydrogen and the surface atoms was determined by a geometry optimization in which all Ti and O atoms were kept fixed at the TiO₂ bulk positions. The effect of saturating the broken surface bonds with the pseudohydrogen atoms on the electronic structure of the surfaces is illustrated in Fig. 4. Without saturation, the LDOS of the fixed Ti(5) and O(2) surface atoms (red dashed lines) deviates strongly from the bulk behavior (black solid lines). The surface band gap is reduced and strong changes and shifts in the LDOS peaks due to the autocompensation can be seen. After saturation of the broken surface bonds, however, the LDOS of the surface atoms (blue dashed-dotted lines) is almost indistinguishable from that of the bulk. With this saturation of the bottom of our slabs we find now also for reduced surface structures a much faster convergence of surface properties with slab thickness. The oscillations in the hydrogen adsorption energy in Fig. 3 have been reduced from 0.1 eV to about 0.02 eV per adsorbed hydrogen atom.

Based on these convergence tests we decided to use for all further calculations slabs with a thickness of four trilayers, including a saturation of the broken surface bonds at the bottom. The upper two trilayers were always fully relaxed, while the atoms in the lower two layers were fixed at the bulk positions. A large (4×2) surface unit cell[73] was used in order to be able to study adequately the coverage dependence of hydrogen and water adsorption. The slab for the stoichiometric surface thus contained 208 atoms, including the artificial atoms for saturating the broken surface bonds at the bottom of the slab. The calculated equilibrium bulk values were taken for the lattice constants parallel to the surface. The slabs were separated by a vacuum region of about 13 Å thickness, which corresponds to the thickness of the slab itself. The surface relaxations of the stoichiometric surface are essentially the same as described by Thompson and Lewis.[57] As shown in Fig. 2, the relaxation energy of the surface is quite substantial. The unrelaxed surface energy is reduced by atomic relaxations from 1.64 eV (1.35 J/m²) by 1.21 eV to 0.43 eV per surface unit cell (0.36 J/m²). For

comparison, the relaxation energy for the ZnO(10$\bar{1}$1) surface amounts to only 0.37 eV per surface unit cell.[74] As we will see later on, these large surface relaxations have a strong impact on the coverage dependence of adsorption energies.

In order to analyze the thermodynamic stability of our different surface structures, we assume that the surfaces can exchange O and H atoms with a surrounding gas phase. Assuming thermodynamic equilibrium, the most stable surface composition at given temperature T and pressure p is given by the minimum of the surface Gibbs free energy $\gamma(T,p)$.[48–51] Since we are only interested in the relative stabilities of surface structures, we calculate directly the difference $\Delta\gamma(T,p)$ in the surface Gibbs free energy between the defective or adsorbate-covered surface and the stoichiometric, ideal surface according to

$$\Delta\gamma(T,p) = \frac{1}{A}\big[G_{slab}^{surf}(T,p,\Delta N_O,\Delta N_H) - G_{slab}^{ref}(T,p)$$
$$+ \Delta N_O\mu_O(T,p) - \Delta N_H\mu_H(T,p)\big], \quad (1)$$

where G_{slab}^{surf} and G_{slab}^{ref} are the Gibbs free energies of the modified and the stoichiometric reference surface configurations, respectively. A is the surface area, ΔN_O and ΔN_H are the differences in the numbers of O and H atoms between the two surfaces, and $\mu_O(T,p)$ and $\mu_H(T,p)$ are chemical potentials representing the Gibbs free energy of the gas phase with which the O and H atoms are exchanged. According to this definition, $\Delta\gamma$ is negative if the modified surface is thermodynamically more stable than the stoichiometric surface and positive otherwise. Assuming that all differences in entropy and volume contributions in $\Delta\gamma$ are negligible,[50,51] we approximate the Gibbs free energies G_{slab}^{surf} and G_{slab}^{ref} by their respective total energies of our DFT slab calculations as usual.[50,51] Upper bounds for the chemical potentials μ_O and μ_H are given by the total energies of their most stable elemental phases,[49] that is, molecular oxygen ($\frac{1}{2}E_{mol}^{O_2}$) and molecular hydrogen ($\frac{1}{2}E_{mol}^{H_2}$), respectively. These upper bounds are taken as zero points of energy by using $\Delta\mu_O=\mu_O-\frac{1}{2}E_{mol}^{O_2}$ and $\Delta\mu_H=\mu_H-\frac{1}{2}E_{mol}^{H_2}$. A lower bound for $\Delta\mu_O$ is given by minus half of the formation energy of bulk TiO₂, i.e., $E_f^{TiO_2}=E_{bulk}^{Ti}+E_{mol}^{O_2}-E_{bulk}^{TiO_2}$ (here $E_{bulk}^{TiO_2}$ and E_{bulk}^{Ti} are the energies of one bulk unit cell of TiO₂ and metallic Ti, respectively),[50,51] for which we have taken the theoretical value of 4.80 eV from our PBE-DFT calculations. The chemical potential can be related to experimental temperature and pressure conditions by using experimental thermochemical reference data or by applying the ideal gas equation.[50,51,59]

The transition state search for the dissociation, desorption, and migration processes was conducted with the nudged-elastic-band (NEB) (Ref. 75) and the dimer methods.[76–79] Fully relaxed configurations were chosen as initial and final states of the NEB calculations. Throughout 12 images were used which were connected by springs with a fixed spring constant of about 20 eV/Å². The two images in the dimer calculations were separated by 0.01 Å in configuration space and the trial steps for translation and rotation were 0.01 Å and 10°, respectively. In all calculations first a good approximation of the transition path was determined with NEB

TABLE I. Vacancy formation energies E_v (in eV) for different oxygen vacancy configurations on TiO_2(110) in the limit of $\Delta\mu_O = 0$ (oxidizing, i.e., oxygen-rich, conditions).

Vacancy type	E_v singlet	E_v triplet
O(2)-v	3.07	3.02
O(3)-v	4.05	4.00
TiO_2-v	1.03	

which was then refined with a dimer method run for a precise location of the transition state.

III. RESULTS AND DISCUSSION

A. Oxygen vacancies on TiO₂(110)

We have investigated three different types of oxygen-related defects. Vacancies are created by removing a single bridging oxygen O(2) atom, a threefold-coordinated O(3) atom from the surface layer, or a full TiO_2 unit of two neighboring bridging O(2) atoms and the underlying Ti cation; see Fig. 1. With our choice of (4×2) supercells this corresponds to a vacancy concentration of 1/8 ML and a defect separation of about 12 Å. The vacancy formation energies for the missing O(2) and O(3) atoms and the TiO_2 unit are given by[80]

$$E_v^O = E_{slab}^{O-v} + \frac{1}{2}E_{mol}^{O_2} - E_{slab}^{ref} + \Delta\mu_O \qquad (2)$$

and

$$E_v^{TiO_2} = E_{slab}^{TiO_2-v} + E_{bulk}^{TiO_2} - E_{slab}^{ref}, \qquad (3)$$

respectively, where E_{slab}^{O-v} and $E_{slab}^{TiO_2-v}$ and E_{slab}^{ref} are the total energies for the defective and the stoichiometric slabs, respectively. The results in Table I show that the O(2) and O(3) vacancies are slightly more stable in the triplet than in the singlet state, in agreement with previous calculations.[24,25,28,30] As one would expect from the local coordination, the formation of an O(2) defect is much more favorable than the O(3) vacancy. Our value for the O(2) vacancy formation energy of 3.02 eV is basically identical to the results of Rasmussen *et al.*[28] (3.03 eV) and Oviedo *et al.*[30] (3.07 eV, singlet state), who both conducted extensive studies on the convergence of $E_v^{O(2)}$ with defect concentration, slab thickness, and the number of relaxed surface layers. Also Ganduglia-Pirovano *et al.*[35] came to the conclusion in their survey of the available literature data that the converged value for the formation energy of isolated O(2) vacancies in GGA-DFT calculations (using the PW91, PBE, or RPBE functional) is about 3.0 eV. This supports that our choice of slab thickness, relaxation, bond saturation at the bottom of the slab, and size of surface unit cell is indeed appropriate to give well-converged results.

In Fig. 5 the vacancy formation energies are plotted as function of the oxygen chemical potential $\Delta\mu_O$ of the environment. Assuming thermodynamic equilibrium of the surfaces with an O_2 gas phase, we have converted the chemical potential into a pressure scale for temperatures of 800 and
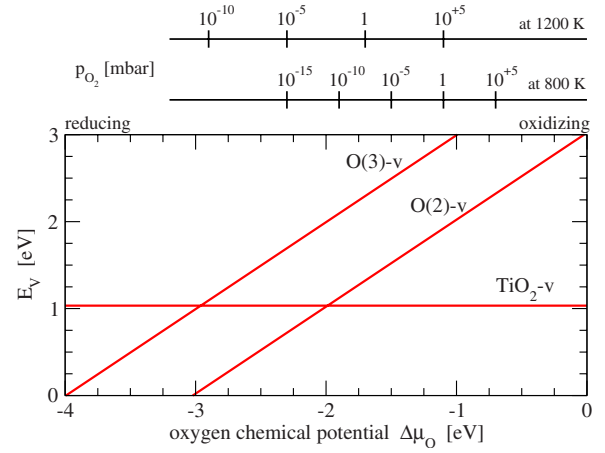

FIG. 5. (Color online) Defect formation energy E_v for O vacancies at the TiO_2(110) surface as function of the oxygen chemical potential $\Delta\mu_O$. In the top x axis, the chemical potential has been translated into a partial pressure scale p_{O_2} of molecular oxygen at 800 and 1200 K.

1200 K using the ideal gas equation.[50,51] Since we have neglected the entropy contributions to the Gibbs free energy of the defective and stoichiometric slabs, we cannot capture with our description the formation of *thermal* oxygen vacancies which are due to the gain in configurational entropy by the random distribution of the defects on the surface. Therefore, at lower temperatures we will always find the stoichiometric, defect-free surface to be the most stable one. We can only predict the appearance of *structural* vacancies which are formed if the gain in entropy by bringing oxygen into the gas phase outweighs the binding energy to the surface. Having this in mind we have to expect that we will overestimate the temperature at which significant amounts of O vacancies (in the percent range) will form. From Fig. 5 we see that at UHV conditions (base pressure of about 10^{-10} mbar) the onset of the formation of structural O(2) vacancies is around 1200 K (i.e., the chemical potential at which the vacancy formation energy E_v becomes zero). This is in quite good agreement with experimental observations,[1] taking into account that an uncertainty of the vacancy formation energy of a few tenths of an eV from the DFT calculations translates into an error bar for this temperature in the range of 100–200 K. Rasmussen *et al.*[28] and Oviedo *et al.*[30] showed that the interaction between the O(2) vacancies is strongly repulsive and that the O vacancy formation energy increases rapidly with higher defect concentrations. Thus, structures with higher O defect concentrations will appear farther to the left in the phase diagram in Fig. 5 so that increasingly reducing conditions are needed to reach defect concentrations beyond a few percent.

On the other hand, quite surprisingly, we find that the formation energy for the TiO_2 defects is much lower than for the O(2) and O(3) vacancies over a wide range of the O chemical potential. Already at temperatures of around 800 K (at UHV conditions), it becomes thermodynamically more favorable to convert the O(2) vacancies into TiO_2 defects. A similar result was recently obtained for the $ZnO(10\bar{1}0)$ surface,[80] where it was found that ZnO dimer vacancies are thermodynamically more stable than O vacancies for most

TABLE II. Adsorption energies E_{ad}^H of H atoms (in eV/atom) on TiO$_2$(110). Configurations with negative values of E_{ad}^H are energetically unstable toward the desorption of H$_2$ molecules. N_H is the number of hydrogen atoms in the (4×2) surface unit cell. The arrangements of the H atoms on the surface are illustrated in Fig. 6.

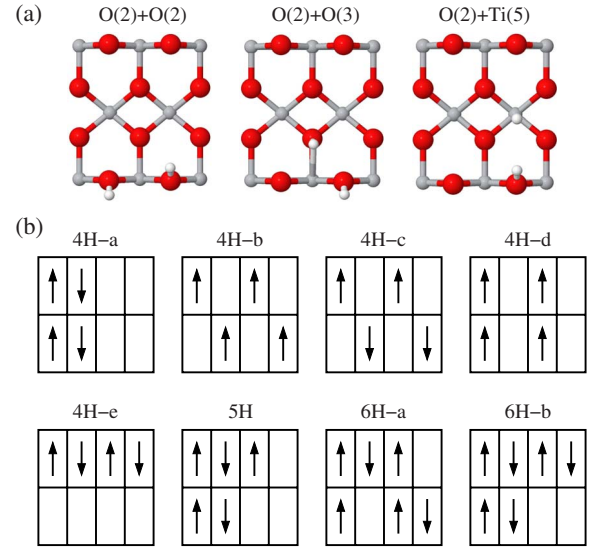| N_H	Configuration	E_{ad}^H
1	O(2)	0.563
	O(3)	−0.062
	Ti(5)	−2.217
2	O(2)+O(2)	0.400
	O(2)+O(3)	0.142
	O(2)+Ti(5)	−0.147
4	4H-a	0.280
	4H-b	0.215
	4H-c	0.211
	4H-d	0.202
	4H-e	0.128
5	5H	0.229
6	6H-a	0.143
	6H-b	0.127
8	8O(2)	0.033
	7O(2)+O(3)	−0.007
	7O(2)+Ti(5)	−0.013
	7O(2)+O$_{sub}^a$	−0.009
	7O(2)+O$_{sub}^b$	−0.012

FIG. 6. (Color online) Schematic illustration of some configurations of the TiO$_2$(110) surface with adsorbed H atoms. (a) Configurations with two adsorbed H atoms. Ti, O, and H atoms are depicted as small gray, large red, and small white spheres, respectively. (b) Configurations with higher H coverage. The arrows indicate the tilt of the OH groups after H adsorption. The corresponding adsorption energies E_{ad}^H are given in Table II.

experimental conditions. While for ZnO a strong suppression of O vacancies on the (10$\bar{1}$0) surface can be expected since Zn has a very low vapor pressure and can easily desorb from the surface (indeed, desorption of Zn is regularly observed in TDS experiments of ZnO), it is more difficult in the case of TiO$_2$ to remove the Ti ions from the surface since the kinetics of the process will play a much larger role. However, one has to consider that the O vacancies, created on the TiO$_2$(110) surface in UHV experiments by annealing, sputtering, or electron bombardment, are only present due to kinetic limitations, and they will be eliminated under ambient conditions not only by a dissociative adsorption of O$_2$ and water, but there is also a strong driving force to transform them into TiO$_2$ vacancies, for example, by a mechanism in which Ti interstitials are created.[81]

B. Hydrogen adsorption on TiO$_2$(110)

In order to investigate the interaction of hydrogen with the TiO$_2$(110) surface, we have calculated the total energies of various hydroxylated TiO$_2$(110) surface structures, taking into account both different hydrogen coverages and adsorption sites for the H atoms. Our results for the hydrogen adsorption energies E_{ad}^H per H atom,

$$E_{ad}^H = \frac{1}{N_H}\left(E_{slab}^{ref} + \frac{N_H}{2}E_{mol}^{H_2} - E_{slab}^{H\text{-}ad}(N_H)\right), \quad (4)$$

where $E_{slab}^{H\text{-}ad}(N_H)$ is the total energy of the slab calculation with N_H adsorbed H atoms, are summarized in Table II.

Single H atoms adsorb preferentially on top of the bridging O(2) atoms, whereas the O(3) and Ti(5) sites are significantly higher in energy. The OH groups, which form upon H adsorption, do not remain upright but break the mirror symmetry of the surface by tilting about 20° (isolated OH groups) and up to 50° (hydroxylation of all bridging O atoms) with respect to the surface normal.

For pairs of H atoms we find that the homolytic adsorption on two neighboring O(2) sites (thereby reducing the surface) is more stable than the heterolytic adsorption on O(2) and Ti(5) [for the atomic configurations, see Fig. 6(a)]. The heterolytic adsorption is even energetically unstable toward desorption of H$_2$. This preference of the homolytic adsorption of hydrogen is expected for an easily reducible oxide. Table II also shows that the interaction between neighboring OH groups is repulsive. The adsorption energy per H atom decreases from 0.56 eV for isolated OH groups to 0.40 eV for neighboring OH pairs.

By comparing the energy of the surface structure with two neighboring OH groups to energy of the structure with an O(2) vacancy, we can directly deduce the energy gain for dissociatively adsorbing a water molecule at isolated O(2) defects by applying a thermodynamic cycle. For the water adsorption energy at O(2) vacancies we find a value of 1.31 eV, which is slightly larger than previously reported results (0.94, 0.97, and 1.10 eV according to Refs. 7, 8, and 82, respectively), but agrees well with an estimated value of about 1.4 eV deduced by a Redhead analysis[83] of a water desorption peak at 520 K in TDS experiment which was assigned to the recombination of neighboring OH groups.[68] According to our NEB calculations this process is without barrier[84] so that the activation energy for desorption is given by the adsorption energy. Since the previous calculations of
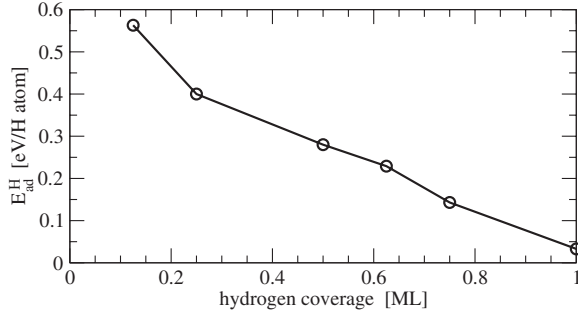
FIG. 7. Hydrogen adsorption energy E_{ad}^H as function of the hydrogen coverage of the surface.

Refs. 7, 8, and 82 were done with (2×2) surface unit cells for which there is still significant interaction between O vacancies and pairs of hydroxyl groups (which can be seen, for example, from our results in Table II), we attribute our slightly higher value for the binding energy of water at O vacancies to our larger (4×2) surface unit cell which represents better-converged results with respect to describing isolated defects and OH pairs. It is interesting to see that we underestimate the binding energy of water in the O vacancies. Since the PBE-DFT calculations tend to overestimate the O vacancy formation energy,[35] this means that also the energy of the reduced surface via hydroxylation is slightly too high. Thus, as in the case of surface reduction via O depletion, also the reducibility of TiO$_2$ via hydrogen adsorption is *underestimated* in the PBE-DFT calculations.

With increasing hydrogen coverage, O(2) remains the preferred adsorption site up to the coverage of a full monolayer. No significant amounts of H atoms will be adsorbed on O(3) and Ti(5) sites. Neighboring OH groups in the [001] direction tend to tilt in opposite directions [see Fig. 6(a)], whereas the coupling between [001] rows (concerning the tilt direction of the OH groups) is relatively weak (with a minor preference of the same tilt direction of OH groups in [1$\bar{1}$0] rows). The ground-state configuration of the fully hydroxylated surface, therefore, will have a (2×1) symmetry. However, since the barrier for flipping the orientation of an OH group is small, they will be fully orientationally disordered at room temperature.

Though O(2) remains to be the preferred adsorption site also with increasing H coverage, the adsorption energy E_{ad}^H per H atom, i.e., the feasibility of further reducing the TiO$_2$(110) surface, decreases strongly upon adsorption of more hydrogen (see Fig. 7). At full monolayer coverage E_{ad}^H is still positive. However, if the interaction energy of hydrogen with the TiO$_2$(110) surface is not expressed as binding energy per H atom but as energy gain per surface area, it becomes obvious from the phase diagram in Fig. 8 that the fully hydroxylated surface is thermodynamically unstable. The surface Gibbs free energy $\Delta\gamma$ for a hydrogen monolayer (this also applies for the 0.75 ML coverage) is higher than the surface energies of lower coverages over the whole range of the hydrogen chemical potential. That is, the energy of the fully hydroxylated surface can be always lowered by desorbing H$_2$ molecules and reducing the H coverage. The highest coverage that can be reached in thermodynamic equilibrium
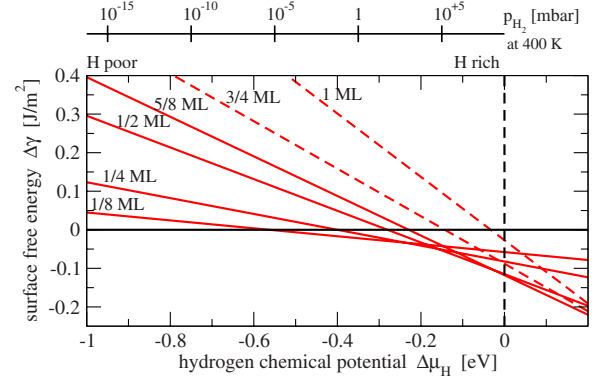

FIG. 8. (Color online) Surface Gibbs free energy $\Delta\gamma$ of TiO$_2$(110) surfaces with different hydrogen coverages as function of the hydrogen chemical potential $\Delta\mu_H$. In the top x axis, the chemical potential has been translated into a partial pressure scale p_{H_2} of molecular hydrogen at 400 K. Thermodynamically unstable surface structures are represented by dashed lines.

in the limit of zero hydrogen chemical potential (i.e., at low temperature and high hydrogen partial pressure) is around 60%–70%. This is in excellent agreement with recent experimental observations where by exposing the TiO$_2$(110) surface to atomic hydrogen no H coverage beyond 70% could be obtained.[21] The experimental setup of exposing the surface to atomic hydrogen is an almost ideal realization of the theoretical assumption underlying the calculation of the phase diagram in Fig. 8, namely, that the surface is in thermodynamic equilibrium with a surrounding H$_2$ gas phase: no kinetic limitations are present and H atoms can adsorb and desorb without encountering any barrier.

In conclusion, this remarkable agreement between theory and experiment suggests that despite the problem of the band gap and the correct position of the defect levels (which we analyzed and discussed in Sec. II), the PBE-DFT calculations seem to be quite able to capture accurately the subtle balance between the energy cost of dissociating H$_2$ molecules versus that of reducing the TiO$_2$(110) surface.

C. Migration of hydrogen atoms

Upon heating the hydroxylated TiO$_2$(110) surface a quite unexpected behavior was observed.[18,21] Monitoring the He atom reflectivity of the surface revealed two distinct maxima at 388 and 625 K (with a small shoulder at 560 K) at which the surface undergoes structural rearrangements. These rearrangements must involve the loss of H atoms since the surface is H free above 650 K. When the Redhead formula[83,85] with a frequency prefactor of 10^{-13} s^{-1} is applied, the two temperatures can be translated (with an uncertainty of about 20%) into activation barriers of 1.03 and 1.68 eV, respectively, for the processes which are involved in the structural changes. In a first assignment the two processes were assumed to be the desorption of hydrogen from the Ti(5) and O(2) sites,[18] respectively. Based on our results on the hydrogen adsorption energy for the different surface sites, however, this interpretation can be clearly ruled out. Surprisingly, in a subsequent conventional TDS measurement, no desorp-

TABLE III. Activation energies E_{act} (in eV) for different migration paths of H atoms on the hydroxylated $TiO_2(110)$ surface. All calculations are based on a fully hydroxylated surface with eight H atoms in the (4×2) surface unit cell. The temperature T_{act} (in K), at which the onset of the processes can be expected, has been estimated from the activation energy E_{act} by applying a standard Redhead analysis (Refs. [83] and [85]) with a frequency factor of 1×10^{13} s^{-1} and a heating rate of 1 K/s.

Migration path	E_{act}	T_{act}
$O(2) \rightarrow O_{sub}^a$	2.56	963 ± 197
$O(3) \rightarrow O_{sub}^a$	0.93	361 ± 72
$Ti(5) \rightarrow O_{sub}^a$	1.52	581 ± 117
$O(2) \rightarrow O(3)$	0.63	248 ± 49
$O(2) \rightarrow Ti(5)$	1.54	588 ± 119
$O(2) \rightarrow O(2)$	1.21	466 ± 93
$2 \times O(2) \rightarrow H_2(gas)$	1.85	703 ± 143

tion of H_2 at all and only a very small amount of water could be detected. This led the authors to the conclusion that instead of desorption taking place, the H atoms migrate into the bulk.[21]

Aiming at identifying the processes which lead to the structural changes in the surface and the loss of the H atoms, we have calculated the activation barriers for different migration paths of H atoms on the hydroxylated $TiO_2(110)$ surface. Some of these migration paths were considered already in a previous DFT study by Yin *et al.*,[21] in which, however, only the smallest possible (1×1) surface unit cell with two adsorbed H atoms was used. In our calculations we start from the fully hydroxylated surface with eight H atoms adsorbed on top of the bridging $O(2)$ atoms in a (4×2) surface unit cell. In the first step we examine how much the energy increases if one of the H atoms from the $O(2)$ sites is placed on top of $O(3)$, $Ti(5)$, or subsurface. As we can see from Table II all three sites are energetically almost degenerate and only about 0.3 eV higher in energy than the $O(2)$ site. (Note that the values in Table II are adsorption energies per H atom. Therefore, to get the energy difference between two structures with different arrangements of the H atoms, the E_{ad}^H values have to be multiplied by the number of adsorbed H atoms, i.e., 8, before subtracting the energies.) This energy difference between the adsorption sites increases when the H coverage decreases. At 1/4 ML H coverage the $O(3)$ and $Ti(5)$ sites are higher in energy by 0.52 and 1.09 eV than the $O(2)$ site, respectively (see Table II).

Returning back to the fully hydroxylated surface we find that the transition barrier for migration of an H atom directly from an $O(2)$ site to a subsurface O atom is quite high (see Table III), whereas diffusion to the $O(3)$ and $Ti(5)$ sites is much more favorable. On the other hand, the activation energies for transferring an H atom from $O(3)$ and $Ti(5)$ to a subsurface O atom are moderate. Overall, the energetically most favorable migration path is from $O(2)$ via $O(3)$ to a subsurface site with barriers of only 0.63 and 0.93 eV, respectively. In contrast, we find for the desorption of H atoms from two neighboring $O(2)$ sites via recombination and formation of H_2 molecules an activation barrier of 1.85 eV. This
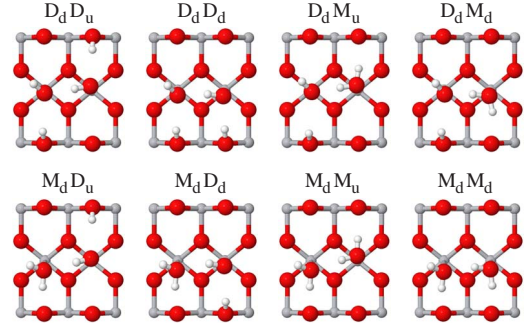

FIG. 9. (Color online) Schematic illustration of water pairs adsorbed on the $TiO_2(110)$ surface. Ti, O, and H atoms are depicted as small gray, large red, and small white spheres, respectively. The labels are defined in Table VI.

implies that it is indeed much easier for the H atoms to diffuse into the bulk instead of desorbing from the surface. The activation barrier of 0.93 eV also corresponds nicely to the temperature of 388 K, at which the onset of structural changes of the hydroxylated $TiO_2(110)$ surface was observed in the HAS experiments.[18] Altogether our results fully support the conclusions of Yin *et al.*[21] that H atoms from a hydroxylated $TiO_2(110)$ surface do not desorb but prefer to migrate into the bulk instead.

D. Water adsorption on $TiO_2(110)$

From the experimental point of view there is a wide consensus that water adsorbs molecularly on defect-free terraces of the $TiO_2(110)$ surface.[1,11–13] In XPS (Ref. [11]) and HREELS (Ref. [12]) measurements only small amounts of dissociated water could be detected under UHV conditions, which may be naturally linked to the presence of residual defects. In TDS (Refs. [11–13]) an intense desorption peak is observed at 270 K which could be attributed to the desorption of a full monolayer of molecularly adsorbed water molecules at Ti^{4+} sites based on XPS, HREELS, and work-function measurements. Interestingly, the peak position shifts to higher temperatures if the initial water coverage Θ is lowered, indicating a repulsive interaction between the adsorbate molecules. This is unusual since for water molecules one would expect an attractive interaction due to the formation of hydrogen bonds, but the same behavior is also observed for the anatase (101) surface.[86] The TDS data could be best described by fitting them to a first-order kinetics model. Activation energies for desorption of $(0.74 - 0.09\Theta)$ eV (Ref. [11]) and $(0.73 - 0.07\Theta)$ eV (Ref. [12]) were obtained, whereas from a modulated molecular-beam study[13] a value of $(0.83 - 0.36\Theta)$ eV was deduced.

On the other hand, over the past years theoretical studies on the adsorption behavior of water on $TiO_2(110)$ came to very contradictory conclusions. In early GGA-DFT studies a much lower adsorption energy for molecular than for dissociative adsorption[38,39] (at full monolayer coverage) was obtained. (It should be noted, however, that the binding energy for the molecular adsorption was underestimated since only a symmetric adsorption of the molecules was considered, which is not the most stable geometry; see Fig. 9.) Subse-

TABLE IV. Literature survey of calculated water adsorption energies E_{ad}^w (in eV/molecule) at monolayer coverage for molecular (mol.), mixed dissociative-molecular (mix.), and dissociative (diss.) adsorptions on TiO_2(110).

Functional	References	E_{ad}^w mol.	E_{ad}^w mix.	E_{ad}^w diss.
BP86[a]	Refs. 38 and 39	0.82		1.08
PW91[b]	Ref. 40	1.13		0.98
PW91[b]	Ref. 41	0.99	1.10	0.91
RPBE[c]	Ref. 44		0.64	0.37
RPBE[c]	Ref. 45	0.52	0.53	0.34
PW91[b]	Ref. 46	1.09	1.05	0.91
PW91[b]	Ref. 47	1.01	0.95	0.90
PBE[d]	This work	0.82	0.77	0.63

[a]References 87 and 88.
[b]Reference 89.
[c]Reference 90.
[d]Reference 54.

quently, Bates *et al.*[40] found a slightly higher adsorption energy for molecular monolayers, whereas Lindan and co-workers[41,44,45] proposed a mixed molecular-dissociated structure as the most stable state. In a Car-Parrinello molecular-dynamics study[43] it was observed that water does not dissociate on the perfect surface, suggesting that the dissociation is hindered by a larger dissociation barrier. Later static calculations of the activation energy for water dissociation supported this point of view.[45] In a quite recent study, however, again molecular adsorption was found to be the most stable adsorption mode not only for water monolayers but even at lower water coverages.[46]

The binding energies E_{ad}^w from these studies for molecular, mixed molecular-dissociative, and full dissociative adsorptions at monolayer coverage are summarized in Table IV. The situation becomes even more confused if the published results for the adsorption of "isolated" water molecules are compared (see Table V). A survey of the publications shows that the results for the water binding energies E_{ad}^w depend sensitively on the computational setup, in particular the slab

thickness and how the results are extrapolated to the limit of infinite slab thickness, as well as on the GGA functional which was used in the calculations (though the result reported in Ref. 7 on the dissociative water adsorption is probably due to an error in the calculations since it was never reproduced in more recent studies). From embedded-cluster calculations using wave-function-based methods (Hartree-Fock, B3LYP, and MP2), it has been suggested that overall GGA-DFT might overestimate the stability of the dissociated state of the water molecules compared to a molecular adsorption.[42] However, embedded-cluster calculations have to be taken with considerable caution. As we will see below, surface re-relaxations, not only of the nearest-neighbor atoms of the adsorption site but also including atoms in the next surface unit cells, make up a major contribution to the binding energy of the molecules, in particular for the dissociated state. Due to the limited cluster size it is questionable how well such structural effects have been captured in this study since the hydroxylated bridging O atoms created by the dissociation of a water molecule were already located at the boundary of the cluster.[42]

The main intention of our study is not to resolve the controversy between the different DFT studies on the molecular or dissociative nature of the adsorption of water, but to evaluate the relative stability of surface hydroxyl groups created by the nonreductive dissociation of water compared to both molecular water adsorption and to hydroxylation of the surface by reductive hydrogen adsorption which we will represent in terms of a phase diagram. The general features of the phase diagram and the qualitative position of the phase boundaries only depend on the overall interaction strength of the water molecules with the TiO_2(110) surface but not, in cases where the energy difference between molecular and dissociative adsorptions is small as for single isolated water molecules, whether the molecular or the dissociated state turns out to be more stable. However, since our calculational setup with a large surface unit cell and a passivated slab seems to be quite reliable to give well-converged results, we explored the question of whether water dissociates on the ideal terraces of the TiO_2(110) surface or not a little bit further than it would have been necessary for the construction of our surface phase diagram.

TABLE V. Literature survey of calculated water adsorption energies E_{ad}^w (in eV/molecule) of isolated molecules for molecular (mol.) and dissociative (diss.) adsorptions on TiO_2(110). The size of the surface unit cell used in the respective calculation is given in the second column. The (2×2) and $c(4 \times 2)$ cells correspond to an effective water coverage of 1/4 ML, whereas a (4×2) cell represents a 1/8 ML water coverage.

Functional	Unit cell	References	E_{ad}^w mol.	E_{ad}^w diss.	ΔE_{ad}
RPBE[a]	(2×2)	Ref. 7	0.56	−0.23	+0.79
RPBE[a]	(2×2)	Ref. 45	0.36	0.56	−0.20
PW91[b]	(2×2)	Ref. 46	0.83	0.71	+0.12
PBE[c]	$c(4 \times 2)$	Ref. 82	0.76	0.66	+0.10
RPBE[a]	(2×2)	Refs. 8 and 9	0.66	0.79	−0.13
PBE[c]	(2×2)	This study	0.82	0.75	+0.07
PBE[c]	(4×2)	This study	0.93	1.04	−0.11

[a]Reference 90.
[b]Reference 89.
[c]Reference 54.

The most favorable adsorption site for water molecules and hydroxyl groups is on top of the fivefold-coordinated Ti(5) cations, thereby restoring their sixfold coordination as in the bulk. Water molecules lie relatively flat on the surface and form a weak hydrogen bond to one of the bridging O(2) atoms. Hydroxyl groups take a more upright position and orient themselves along a Ti(5)-O(3) bond, as long as they cannot form a hydrogen bond to an adsorbed molecule on a neighboring Ti(5) site (see Fig. 9).

For single water molecules in a (4×2) surface unit cell, we find that dissociative adsorption is preferred compared to the molecular state by 0.11 eV, as can be seen from the compiled results in Table VI. This is in contrast to the results of Refs. 7, 46, and 82, but in agreement with Refs. 8, 9, and 45. On the other hand, at full monolayer coverage molecular adsorption is found to be 0.05 or 0.19 eV per water molecule more stable than partial or full dissociation, respectively. In view of the very contradictory results from previous DFT calculations in the literature on the relative stability of the molecular and dissociative adsorption modes of water on TiO$_2$(110), we have carefully re-evaluated the convergence of our computational setup. From the survey of the literature it appears that the slab thickness and the degree of atomic relaxation of the slabs are the most crucial parameters. Therefore we have recalculated the energy difference ΔE_{ad} between molecular and dissociative adsorptions of water as a function of slab thickness. In the first set of calculations we have considered a full monolayer water coverage as represented by one water molecule in a (1×1) surface unit cell. As shown in Fig. 10, the molecular and dissociative adsorption energies E_{ad}^{mol} and E_{ad}^{diss}, respectively, exhibit the well-known strong odd-even oscillations if the water molecules are adsorbed symmetrically on both sides of the slab and a full atomic relaxation is performed. These oscillations are even present in the energy difference $\Delta E_{ad} = E_{ad}^{mol} - E_{ad}^{diss}$. Switching to our standard setup in which we adsorb water only on one side of the slab, fix the atoms in the two bottom layers at the bulk positions, and saturate the broken surface bonds at the bottom with pseudohydrogen atoms, the odd-even oscillations are almost completely removed (see Fig. 10). For ΔE_{ad} we find only a small increase from 0.19 eV for the four-trilayer slab to 0.23 eV in the limit of infinite slab thickness. In the second set of calculations we repeated the calculations for a single water molecule in a (4×2) surface unit cell with our passivated slabs for slab thicknesses of up to seven trilayers. In the seven-trilayer calculation the supercell contained 355 atoms. Also in this case, as shown in Fig. 10, there are almost no odd-even oscillations visible in the water adsorption energy E_{ad} and the energy difference ΔE_{ad} between the molecular and dissociative adsorptions increases only slightly from −0.11 eV for four trilayers to −0.06 eV in the six- and seven-trilayer calculations. Since in general such small energy differences depend sensitively on the quality of the pseudopotentials and the functional which are used in the computations, we only conclude that molecular and dissociative adsorptions become energetically degenerate in the limit of single isolated water molecules.

When comparing our results on the adsorption of isolated water molecules with the literature survey in Table V, it has to be taken into account that in the previous calculations for

TABLE VI. Water adsorption energies E_{ad}^w (in eV/molecule) on TiO$_2$(110) for different coverages taking into account molecular (M) and dissociated (D) states of the water molecules with downward (d) or upward (u) orientation. N_w is the number of water molecules in the (4×2) surface unit cell. Parentheses denote pairs of water molecules as illustrated in Fig. 9. The structures with four water molecules consist of two water pairs filling one [001] row and leaving every second one empty. At full monolayer coverage, both [001] rows are equally filled with water pairs. The periodicity of the resulting structure is reported in the "Config." column.

N_w	Config.	E_{ad}^w
1	Single water	
	D$_d$	1.04
	M$_d$	0.93
2	Single water	
	2D$_d$-$c(4 \times 2)$	0.97
	2D$_d$-$p(4 \times 1)$	0.96
	2D$_d$-$p(2 \times 2)$	0.75
	2M$_d$-$c(4 \times 2)$	0.83
	2M$_d$-$p(4 \times 1)$	0.82
	2M$_d$-$p(2 \times 2)$	0.80
	Water pairs	
	(D$_d$D$_u$)	0.94
	(D$_d$D$_d$)	0.90
	(D$_d$M$_u$)	0.97
	(D$_d$M$_d$)	0.96
	(M$_d$D$_u$)	0.90
	(M$_d$D$_d$)	0.88
	(M$_d$M$_u$)	0.88
	(M$_d$M$_d$)	0.90
4	Double pairs along [001]	
	2(D$_d$D$_u$)-(2×2)	0.67
	2(D$_d$D$_d$)-(1×2)	0.64
	2(D$_d$M$_u$)-(2×2)	0.81
	2(D$_d$M$_d$)-(2×2)	0.80
	2(M$_d$M$_u$)-(2×2)	0.84
	2(M$_d$M$_d$)-(1×2)	0.86
8	Quadruple pairs	
	4(D$_d$D$_u$)-(2×1)	0.61
	4(D$_d$D$_d$)-(1×1)	0.63
	4(D$_d$M$_u$)-(2×1)	0.77
	4(D$_d$M$_d$)-(2×1)	0.77
	4(M$_d$M$_u$)-(2×1)	0.80
	4(M$_d$M$_d$)-(1×1)	0.82

"single" water molecules smaller surface unit cells with effective water coverages of 1/4 ML were used, compared to 1/8 ML in our study. As can be seen from our results in Table VI, at 1/4 ML coverage there is already a significant interaction between the water molecules. For two water molecules in the (4×2) surface unit cell the water binding energy is clearly reduced compared to that for a single molecule. The reason is, as we will point out below, the large contribution
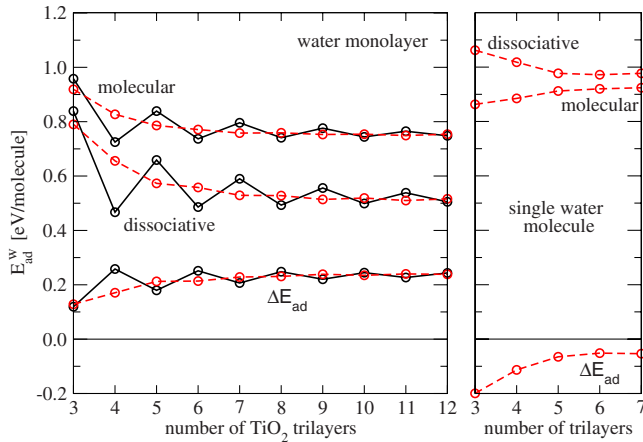
FIG. 10. (Color online) Convergence of the molecular and dissociative water adsorption energies, E_{ad}^w, and the difference $\Delta E_{ad} = E_{ad}^{mol} - E_{ad}^{diss}$ with slab thickness at full monolayer coverage (left) and for single water molecules in a (4×2) surface unit cell (right). The solid black lines represent results from full relaxations with water adsorbed symmetrically on both sides of the slab. The calculations in which water was adsorbed only on one side of the slab with the bottom two trilayers fixed at the bulk positions and the broken surface bonds at the bottom of the slab saturated with pseudohydrogen atoms are shown by the red dashed lines.

of the surface relaxations to the binding energy, which is now smaller since less degrees of freedom are associated with each molecule. In particular, for a (2×2) arrangement of water molecules, which was used in basically all previous calculations as setup for isolated molecules, we find already a preference for molecular adsorption. Clearly, the 1/4 ML coverage does not represent isolated water molecules, and in principle, it would have to be checked if our 1/8 ML truly represents the limit of independent molecules. This implies that also in the embedded-cluster approach large clusters are needed to take these contributions from the atomic relaxations appropriately into account.

Our result that the molecular and dissociative adsorption modes for isolated water molecules are energetically degenerate is not in agreement with the common view expressed in most experimental studies that water only dissociates at defect sites. Since our calculations are very well converged, this might point toward a deficiency of the pseudopotential approximation or, in general, PBE-DFT calculations. However, it also has to be taken into account that all experiments have shown a certain amount of dissociated molecules and it is very difficult to distinguish whether they only stem from dissociation at defects or if some initial dissociation at very low coverages has taken place.

Comparing the water binding energies of two water molecules in a $c(4 \times 2)$ arrangement with those in the $p(4 \times 1)$ configuration, we find that the interaction of water molecules between different [001] rows is rather weak since the relative position of the water molecules within the [001] rows does not matter. This is very different from the situation when both water molecules are placed into the same [001] row [as in the $p(2 \times 2)$ configuration], where the changes in the surface relaxation lead to a strong repulsion between dissociated molecules. This repulsion was also reported by Lindan and

Zhang,[45] although with a slightly smaller magnitude. The repulsion can be compensated for by adsorbing the two water molecules on neighboring Ti(5) sites, since now a hydrogen bond between the molecules is formed. We have considered all possible pairs of dissociated and undissociated water molecules with "upward" and "downward" orientations as illustrated in Fig. 9. As can be inferred from the binding energies in Table VI, all these configurations are almost equivalent, with a slight preference of pairs of dissociated/undissociated molecules in which the donating molecule of the hydrogen bond stays intact and the receiving molecule dissociates. Furthermore, we can see that the relative orientation of the molecules within the pair (upward or downward) does not matter, which will be also true at higher water coverages.

We take now these water pairs as building blocks to form higher water coverages. First we put two water pairs in the same [001] row to build structures of alternating full and empty [001] lines. The molecular adsorption is now the most stable one. The half-dissociated structure of Lindan *et al.*[41] is only slightly lower in energy. The fully dissociated structure, however, has become clearly unfavorable. Since the interaction of the water molecules between [001] rows is weak, as already pointed out above, this result remains unchanged when all [001] rows are filled with water molecules and the full monolayer coverage is reached.

For the length of the Ti(5)-O$_{water}$ bond we obtained values between 2.246 and 2.306 Å for isolated water molecules and at full monolayer coverage, respectively. In a recent quantitative analysis of photoelectron diffraction experiments[92] a value for this bond length of 2.21 ± 0.02 Å was determined. Taking into account that GGA typically overestimates bond length by 1–2 %, our result for isolated water molecules agrees quite well with the experimental value, but is overestimated slightly in the limit of full monolayer coverage.

In conclusion, we find that in the limit of very low coverages the molecular and dissociative adsorption modes of water are almost degenerate. For single isolated water molecules we find a small preference for dissociation. However, at coverages when first water pairs are formed, mixed dissociated-molecular structures are more favorable than full dissociation. Finally, in the full monolayer coverage limit the molecular adsorption is the most stable configuration. Based on these results one would expect that if water islands are formed upon adsorption, almost all water molecules stay intact and only those molecules at the boundary of the water patch which do not have a neighbor to which they can form a hydrogen bond may dissociate. It is interesting to see the difference in the role of donated and accepted hydrogen bonds for the stability of water molecules between the TiO$_2$(110) and ZnO(10$\bar{1}$0) surface. On ZnO(10$\bar{1}$0), water molecules also show a tendency to dissociate.[93–95] But while on ZnO(10$\bar{1}$0) isolated water molecules stay intact and only start to dissociate when they receive a hydrogen bond, isolated water molecules on TiO$_2$(110) are found to be close to dissociation, and recombination is preferential when they can donate a hydrogen bond.

Our results for the water binding energies are throughout slightly lower than the previous results obtained with the PW91 functional,[40,41,46,47] but significantly higher than what

has been found in RPBE calculations[7–9,44,45,82] (see also Tables IV and V). In order to compare our water binding energy of 0.82 eV at full monolayer coverage with experiment, we have furthermore calculated the corrections due to the zero-point vibration energy (ZPE). The vibration frequencies of the surface with and without the molecular water monolayer were obtained in harmonic approximation by a finite difference scheme. Only the atoms in the adsorbate and the first surface layer were displaced by 0.01 Å in the three Cartesian directions. For the ZPE we obtain 0.12 eV so that we arrive at a ZPE-corrected water binding energy at monolayer coverage of 0.70 eV, which is in excellent agreement with the results of the TDS experiments of 0.65 eV (Ref. 11) and 0.66 eV (Ref. 12). The minor overbinding of the water molecules is typical of PBE calculations and has also been observed for the adsorption of water on $ZnO(10\bar{1}0)$, where PBE calculations gave a water binding energy of 1.13 eV (without ZPE corrections) compared to the TDS-Redhead analysis of 1.03 eV.[93]

Looking at the qualitative trend of the adsorption energy with water coverage of the surface, it is interesting to see in Table VI that overall the binding energy decreases with water saturation. This contradicts the results of Ref. 46, whereas it is in full agreement with the RPBE calculations of Lindan and Zhang[44,45] and, in addition, to the experimental observation in the TDS measurements. This is a rather unusual behavior since one would expect an increase in the binding energy with water coverage due to the formation of hydrogen bonds. In order to gain deeper insights into the origin of this behavior, we have decomposed the process of desorbing the water molecules into four steps. Starting from the fully relaxed adsorbate structure we detach in the first step the water layer from the surface without relaxing the atoms. Then we separate the water molecules in order to obtain the hydrogen bond strength. Finally, we allow the $TiO_2(110)$ surface and the water molecules to relax to obtain the relaxation energies of the systems [see Ref. 95 for a similar analysis of the water adsorption energy on $ZnO(10\bar{1}0)$]. For structures with neighboring water molecules we find indeed that hydrogen bonds are formed, which increases the water binding energy. This gain in adsorption energy, however, is overcompensated at higher coverages by a loss in relaxation energy of the substrate per adsorbate molecule. Why are the surface relaxations so much more important for the $TiO_2(110)$ surface than, for example, $ZnO(10\bar{1}0)$? As we have seen in Sec. II, the surface relaxation energy of the stoichiometric, ideal surface is quite large, 1.21 eV per surface unit cell, compared to 0.37 eV for $ZnO(10\bar{1}0)$. Thus, re-relaxations induced by the restoration of the cation bulk coordination upon water adsorption have a much stronger impact on the binding energy of the molecules than for $ZnO(10\bar{1}0)$.

Lindan and Zhang[45] suggested that the dissociation of water at low coverages had not been observed experimentally because the dissociation of the molecules is hindered by a significant dissociation barrier which is difficult to overcome on the time scale of the experiments. Using NEB with a subsequent refinement of the transition state with the dimer method, we have calculated the activation barrier for water dissociation for two cases: an isolated water molecule in a
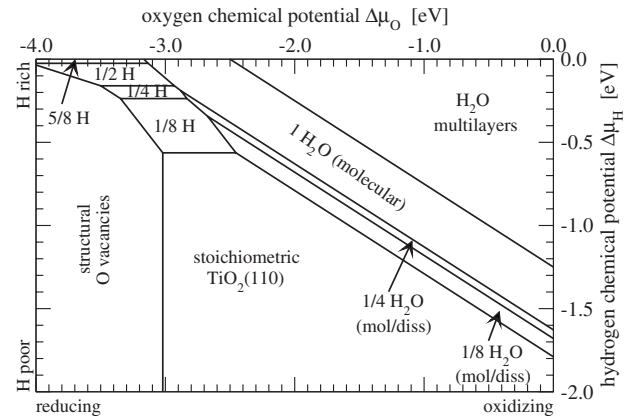

FIG. 11. Phase diagram for the $TiO_2(110)$ surface in thermodynamic equilibrium with H_2 and O_2 particle reservoirs controlling the chemical potentials $\Delta\mu_H$ and $\Delta\mu_O$.

(4×2) surface cell and a single water molecule within a molecularly adsorbed water layer [also employing a (4×2) supercell]. Our results of 0.16 and 0.14 eV, respectively, are significantly lower than the activation barriers reported by Lindan and Zhang[45] of 0.45 eV [single water molecule in a (4×1) cell] and 0.26 eV (dissociation of every second water molecule in a full monolayer) and show a much weaker dependence on the water coverage. Therefore, based on our results, we cannot confirm that the dissociation of water molecules at low coverages is prevented by a large dissociation barrier.

E. Surface phase diagram

Finally we combine the results of Secs. III A–III D to construct a two-dimensional phase diagram. We assume that the $TiO_2(110)$ surface is simultaneously in thermodynamic equilibrium with reservoirs with which it can exchange O and H atoms, for example, a surrounding O_2 and H_2 gas phase. The surface free energy $\Delta\gamma$ of the different $TiO_2(110)$ surface structures now depends on both chemical potentials, $\Delta\mu_O$ and $\Delta\mu_H$. By indicating the most stable structure and composition of the $TiO_2(110)$ surface as a function of the two chemical potentials, we obtain the phase diagram which is shown in Fig. 11.

The surface phase diagram of Fig. 11 summarizes in a condensed fashion the results of our study on the relative stabilities of the different surface compositions which we have considered. The phase diagram is dominated by four different types of surface structures: the stoichiometric, ideal surface; the water-saturated, oxidized surface; and the reduced surface structures by O depletion and H adsorption. For ambient conditions we find that the $TiO_2(110)$ surface is saturated with molecularly adsorbed water. The water can be gradually removed by lowering the O and H chemical potentials (i.e., by heating or lowering the partial pressures). Passing through a transition region with low water coverages in which dissociated water molecules may appear, the stoichiometric, ideal surface structure is reached. It is the most stable surface structure at UHV conditions for a wide range of temperatures. By heating the surface in UHV, the surface can be

reduced by removing bridging oxygen atoms and creating structural O vacancies. At hydrogen-rich and oxygen-poor conditions the surface is reduced by hydrogen adsorption. However, the surface cannot be fully hydroxylated, but only a maximum H coverage of about 60% can be reached.

Overall the surface phase diagram shows a quite expected behavior of the $TiO_2(110)$ surface and does not yield any new surprises. Under UHV conditions the stoichiometric and the O-reduced surface structures are the most important ones. On the other hand, under wet conditions or at high hydrogen partial pressures, as it is typical in catalytic or photochemical applications, the surface is water covered or reduced via hydroxylation.

IV. SUMMARY AND CONCLUSIONS

Using density-functional theory we have investigated in detail the formation of oxygen-related vacancies as well as the interaction of hydrogen and water with the $TiO_2(110)$ surface in terms of a comprehensive surface phase diagram. Careful convergence tests have shown that a computational setup of using slabs consisting of four trilayers in conjunction with saturating the surface bonds at the bottom with artificial hydrogenlike atoms with effective nuclear charges of $+4/3$ and $+2/3$ and fixing the atoms in the bottom two trilayers at their bulk positions almost completely eliminates the otherwise pronounced odd-even oscillations of surface and adsorption energies as a function of slab thickness. Using this procedure, the relaxation energy of the stoichiometric surface and the H and H_2O adsorption energies at full monolayer coverage are within 0.06 eV per surface unit cell, 0.02 eV per H atom, and 0.04 eV per H_2O molecule, respectively, of the extrapolated results for infinitely thick slabs. Thus, very well-converged results with slab thickness are obtained without relying on somewhat questionable extrapolation schemes such as the "25% rule"[46] or averaging four- and five-trilayer results,[30] as proposed previously in the literature.

It is also demonstrated that the contributions of surface relaxations to both binding and formation energies of molecules and defects, respectively, are substantial. Both adsorbate- and defect-induced relaxations are not limited to one surface unit cell, but contributions to the relaxation energy from more neighboring surface cells have to be taken into account. This leads to substrate-mediated interactions between defects and adsorbate molecules which can extend over several lattice constants. Consequently, large surface unit cells have to be used when properties of isolated defects or adsorbed molecules are studied. The same arguments apply for embedded-cluster studies where clusters have to be large enough to be able to take the relaxations of the relevant environment appropriately into account.

In general, GGA-DFT calculations of reduced TiO_2 structures are hampered by the underestimation of the TiO_2 band gap of about 1.0 eV. For isolated O vacancies and pairs of OH groups on the $TiO_2(110)$ surface, it has been shown that in GGA-DFT calculations the defect level lies at the bottom of the conduction band[35,67] instead of 0.7–0.9 eV below. Naively one would therefore expect that GGA-DFT calculations

should underestimate the energy of reduced TiO_2 structures and thus *overestimate* the reducibility of TiO_2 since defect states will tend to be too delocalized. In contrast to this expectation, a survey of the literature data showed instead that GGA-DFT overestimates the O vacancy formation energy. Furthermore we found in the present study that the dissociation energy of water at O vacancies is slightly too low in the PBE-DFT calculations and also the predicted maximum coverage of the $TiO_2(110)$ surface with hydrogen atoms is found to be slightly smaller than observed in experiment. This implies that in all three cases the GGA-DFT calculation have *underestimated* the reducibility of the $TiO_2(110)$ surface. However, the presumable error in the total energies is small: about 0.3 eV for the O defect formation energy and 0.1 eV in the other two cases. Based on this analysis we conclude that the *energetics* is quite reliably described by GGA-DFT despite the problem of such calculations of obtaining accurately the underlying electronic structure of the corresponding reduced TiO_2 surfaces. It might be argued that the energetics of reduced TiO_2 is well described because, although the defect level of O vacancies and OH pairs is at the bottom of the conduction band instead of 0.7–0.9 eV below, its energy difference with respect to the top of the valence band is almost right. This might be correct for single isolated O vacancies and OH pairs. However, in the case of an increasing hydroxylation of the surface when the defect states start to interact and to hybridize with the conduction band, the whole defect band is now more easily accessible due to the underestimation of the band gap, but still the overall energetics is quite reliable with a tendency to *underestimate* the reducibility of TiO_2.

After having clarified these crucial convergence and accuracy issues, we have compared the relative stabilities of surfaces with oxygen vacancies or adsorbed hydrogen atoms and water molecules by combining our DFT calculations with a thermodynamic formalism. Lowest-energy structures were determined by assuming that the surfaces are in thermodynamic equilibrium with oxygen and hydrogen reservoirs. The exchange of O and H atoms with the reservoirs is described by introducing appropriate chemical potentials which can be related to experimental temperature and pressure conditions. This allows us to extend the zero-temperature and zero-pressure DFT calculations to more realistic environmental conditions such as in UHV surface science experiments or in catalytic and photochemical applications.

The central result of this approach is the phase diagram depicted in Fig. 11. For ambient conditions we find that the nonreductive adsorption of water prevails. A full monolayer of molecularly adsorbed water is predicted as the most stable adsorbate structure, in agreement with experimental observations. In the low-coverage limit molecular and dissociative adsorptions become energetically degenerate. In addition, according to our calculations the dissociation barrier for molecularly adsorbed water molecules is not large enough to prevent their dissociation even at low temperatures.

At strongly reducing, oxygen-poor conditions structural O vacancies are formed on the $TiO_2(110)$ surface in thermodynamic equilibrium. However, for a wide range of temperature and pressure conditions it is found that removing full

TiO$_2$ units is thermodynamically more favorable instead. In the case of reduction of the surface via hydrogen adsorption, we observed that the surface cannot be fully hydroxylated in thermodynamic equilibrium. A maximum coverage of about 60% is predicted from our thermodynamical analysis. Furthermore, our calculated energy barriers for hydrogen migration indicate than hydrogen atoms rather migrate into the bulk than desorbing from the surface. Both observations are supported by recent experiments in which a maximum saturation of the surface with hydrogen of 70% is reported, whereas no desorption of H$_2$ could be observed in TDS.[21]

[1] U. Diebold, Surf. Sci. Rep. **48**, 53 (2003).

[2] M. Ramamoorthy, D. Vanderbilt, and R. D. King-Smith, Phys. Rev. B **49**, 16721 (1994).

[3] S. J. Tauster, S. C. Fung, and R. L. Garten, J. Am. Chem. Soc. **100**, 170 (1978).

[4] S. J. Tauster, Acc. Chem. Res. **20**, 389 (1987).

[5] M. A. Vannice and C. Sudhakar, J. Phys. Chem. **88**, 2429 (1984).

[6] I. M. Brookes, C. A. Muryn, and G. Thornton, Phys. Rev. Lett. **87**, 266103 (2001).

[7] R. Schaub, P. Thostrup, N. Lopez, E. Lægsgaard, I. Stensgaard, J. K. Nørskov, and F. Besenbacher, Phys. Rev. Lett. **87**, 266104 (2001).

[8] S. Wendt, R. Schaub, J. Matthiesen, E. K. Vestergaard, E. Wahlström, M. D. Rasmussen, P. Thorstrup, L. M. Molina, E. Lægsgaard, I. Stensgaard, B. Hammer, and F. Besenbacher, Surf. Sci. **598**, 226 (2005).

[9] S. Wendt, J. Matthiesen, R. Schaub, E. K. Vestergaard, E. Lægsgaard, F. Besenbacher, and B. Hammer, Phys. Rev. Lett. **96**, 066107 (2006).

[10] O. Bikondoa, C. L. Pang, R. Ithnin, C. A. Muryn, H. Onishi, and G. Thornton, Nature Mater. **5**, 189 (2006).

[11] M. B. Hugenschmidt, L. Gamble, and C. T. Campbell, Surf. Sci. **302**, 329 (1994).

[12] M. A. Henderson, Surf. Sci. **355**, 151 (1996).

[13] D. Brinkley, M. Dietrich, T. Engel, P. Farrall, G. Gantner, A. Schafer, and A. Szuchmacher, Surf. Sci. **395**, 292 (1998).

[14] J.-M. Pan, B. L. Maschhoff, U. Diebold, and T. E. Madey, J. Vac. Sci. Technol. A **10**, 2470 (1992).

[15] M. Batzill, K. Katsiev, J. M. Burst, U. Diebold, A. M. Chaka, and B. Delley, Phys. Rev. B **72**, 165414 (2005).

[16] K. Katsiev, M. Batzill, U. Diebold, A. Urban, and B. Meyer, Phys. Rev. Lett. **98**, 186102 (2007).

[17] V. E. Henrich and R. L. Kurtz, Phys. Rev. B **23**, 6280 (1981).

[18] M. Kunat, U. Burghaus, and Ch. Wöll, Phys. Chem. Chem. Phys. **6**, 4203 (2004).

[19] S. Suzuki, K. I. Fukui, H. Onishi, and Y. Iwasawa, Phys. Rev. Lett. **84**, 2156 (2000).

[20] T. Fujino, M. Katayama, K. Inudzuka, T. Okuno, and K. Oura, Appl. Phys. Lett. **79**, 2716 (2001).

[21] X.-L. Yin, M. Calatayud, H. Qiu, Y. Wang, A. Birkner, C. Minot, and Ch. Wöll, ChemPhysChem **9**, 253 (2008).

[22] M. Ramamoorthy, R. D. King-Smith, and D. Vanderbilt, Phys. Rev. B **49**, 7709 (1994).

[23] P. J. D. Lindan, N. M. Harrison, M. J. Gillan, and J. A. White, Phys. Rev. B **55**, 15919 (1997).

[24] A. T. Paxton and L. Thien-Nga, Phys. Rev. B **57**, 1579 (1998).

[25] T. Bredow and G. Pacchioni, Chem. Phys. Lett. **355**, 417 (2002).

[26] A. Vijay, G. Mills, and H. Metiu, J. Chem. Phys. **118**, 6536 (2003).

[27] X. Wu, A. Selloni, M. Lazzeri, and S. K. Nayak, Phys. Rev. B **68**, 241402(R) (2003).

[28] M. D. Rasmussen, L. M. Molina, and B. Hammer, J. Chem. Phys. **120**, 988 (2004).

[29] X. Wu, A. Selloni, and S. K. Nayak, J. Chem. Phys. **120**, 4512 (2004).

[30] J. Oviedo, M. A. San Miguel, and J. F. Sanz, J. Chem. Phys. **121**, 7427 (2004).

[31] S.-G. Wang, X.-D. Wen, D.-B. Cao, Y.-W. Li, J. Wang, and H. Jiao, Surf. Sci. **577**, 69 (2005).

[32] Y.-F. Zhang, W. Lin, Y. Li, K.-N. Ding, and J.-Q. Li, J. Phys. Chem. B **109**, 19270 (2005).

[33] K. Hameeuw, G. Cantele, D. Ninno, F. Trani, and G. Iadonisi, Phys. Status Solidi A **203**, 2219 (2006).

[34] T. Pabisiak and A. Kiejna, Solid State Commun. **144**, 324 (2007).

[35] M. V. Ganduglia-Pirovano, A. Hofmann, and J. Sauer, Surf. Sci. Rep. **62**, 219 (2007).

[36] J. Leconte, A. Markovits, M. K. Skalli, C. Minot, and A. Belmajdoub, Surf. Sci. **497**, 194 (2002).

[37] R. L. Kurtz, R. Stockbauer, T. E. Madey, E. Roman, and J. L. De Segovia, Surf. Sci. **218**, 178 (1989).

[38] J. Goniakowski and M. J. Gillan, Surf. Sci. **350**, 145 (1996).

[39] P. J. D. Lindan, N. M. Harrison, J. M. Holender, and M. J. Gillan, Chem. Phys. Lett. **261**, 246 (1996).

[40] S. P. Bates, G. Kresse, and M. J. Gillan, Surf. Sci. **409**, 336 (1998).

[41] P. J. D. Lindan, N. M. Harrison, and M. J. Gillan, Phys. Rev. Lett. **80**, 762 (1998).

[42] E. V. Stefanovich and T. N. Truong, Chem. Phys. Lett. **299**, 623 (1999).

[43] W. Langel, Surf. Sci. **496**, 141 (2002).

[44] C. Zhang and P. J. D. Lindan, J. Chem. Phys. **118**, 4620 (2003).

[45] P. J. D. Lindan and C. Zhang, Phys. Rev. B **72**, 075439 (2005).

[46] L. A. Harris and A. A. Quong, Phys. Rev. Lett. **93**, 086105 (2004); P. J. D. Lindan and C. Zhang, *ibid.* **95**, 029601 (2005); L. A. Harris and A. A. Quong, *ibid.* **95**, 029602 (2005).

[47] H. Perron, J. Vandenborre, C. Domain, R. Drot, J. Roques, E. Simoni, J.-J. Ehrhardt, and H. Catalette, Surf. Sci. **601**, 518 (2007).

[48] E. Kaxiras, Y. Bar-Yam, J. D. Joannopoulos, and K. C. Pandey, Phys. Rev. B **35**, 9625 (1987).

[49] G.-X. Qian, R. M. Martin, and D. J. Chadi, Phys. Rev. B **38**, 7649 (1988).

[50] K. Reuter and M. Scheffler, Phys. Rev. B **65**, 035406 (2001).

[51] B. Meyer, Phys. Rev. B **69**, 045416 (2004).

[52] R. Car and M. Parrinello, Phys. Rev. Lett. **55**, 2471 (1985).

[53] D. Marx and J. Hutter, in *Modern Methods and Algorithms of Quantum Chemistry*, edited by J. Grotendorst (NIC, FZ Jülich, 2000), p. 301 (see www.theochem.rub.de/go/cprev.html); J. Hutter *et al.*, CPMD code (see www.cpmd.org).

[54] J. P. Perdew, K. Burke, and M. Ernzerhof, Phys. Rev. Lett. **77**, 3865 (1996); **78**, 1396(E) (1997).

[55] D. Vanderbilt, Phys. Rev. B **41**, 7892 (1990).

[56] T. Bredow, L. Giordano, F. Cinquini, and G. Pacchioni, Phys. Rev. B **70**, 035419 (2004).

[57] S. J. Thompson and S. P. Lewis, Phys. Rev. B **73**, 073403 (2006).

[58] S. C. Abrahams and J. L. Bernstein, J. Chem. Phys. **55**, 3206 (1971).

[59] I. G. Batyrev, A. Alavi, and M. W. Finnis, Phys. Rev. B **62**, 4698 (2000).

[60] This deviation is due to the O pseudopotential. By decreasing the cutoff radius, making the local part of the potential more attractive, and adding d projectors, the converged all-electron result for the O_2 binding energy can be systematically approached. However, such pseudopotentials are usually much harder and require a larger plane-wave cutoff energy.

[61] NIST Standard Reference Database No. 69 in *NIST Chemistry WebBook*, edited by P. J. Linstrom and W. G. Mallard (National Institute of Standards and Technology, Gaithersburg, MD, 2001) (see http://webbook.nist.gov).

[62] G. Pacchioni, J. Chem. Phys. **128**, 182505 (2008).

[63] K. M. Glassford and J. R. Chelikowsky, Phys. Rev. B **46**, 1284 (1992).

[64] J. Pascual, J. Camassel, and H. Mathieu, Phys. Rev. Lett. **39**, 1490 (1977); Phys. Rev. B **18**, 5606 (1978).

[65] W. Göpel, J. A. Anderson, D. Frankel, M. Jaehnig, K. Phillips, J. A. Schäfer, and G. Rocker, Surf. Sci. **139**, 333 (1984).

[66] M. A. Henderson, Surf. Sci. **400**, 203 (1998).

[67] C. Di Valentin, G. Pacchioni, and A. Selloni, Phys. Rev. Lett. **97**, 166803 (2006).

[68] M. A. Henderson, W. S. Epling, C. H. F. Peden, and C. L. Perkins, J. Phys. Chem. B **107**, 534 (2003).

[69] K. J. Hameeuw, G. Cantele, D. Ninno, F. Trani, and G. Iadonisi, J. Chem. Phys. **124**, 024708 (2006).

[70] A. Kiejna, T. Pabisiak, and S. W. Gao, J. Phys.: Condens. Matter **18**, 4207 (2006).

[71] M. Lannoo and P. Friedel, *Atomic and Electronic Structure of Surfaces* (Springer, Berlin, 1991).

[72] B. Meyer and D. Marx, Phys. Rev. B **69**, 235420 (2004).

[73] We follow here the notation of Ref. 1: an ($n \times m$) cell is built by repeating the primitive surface unit cell n and m times along the bulk [001] and [$1\bar{1}0$] directions, respectively. It has dimensions of $nc \times m\sqrt{2}a$. In some other publications the order of n and m is reversed.

[74] B. Meyer and D. Marx, Phys. Rev. B **67**, 035403 (2003).

[75] H. Jónsson, G. Mills, and K. W. Jacobsen, in *Classical and Quantum Dynamics in Condensed Phase Simulations*, edited by B. J. Berne, G. Ciccotti, and D. F. Coker (World Scientific, Singapore, 1998), p. 385.

[76] G. Henkelman and H. Jónsson, J. Chem. Phys. **111**, 7010 (1999).

[77] G. Henkelman, B. P. Uberuaga, and H. Jónsson, J. Chem. Phys. **113**, 9901 (2000).

[78] G. Henkelman and H. Jónsson, J. Chem. Phys. **113**, 9978 (2000).

[79] A. Heyden, A. T. Bell, and F. J. Keil, J. Chem. Phys. **123**, 224101 (2005).

[80] R. Kováčik, B. Meyer, and Dominik Marx, Angew. Chem. **119**, 4980 (2007); Angew. Chem., Int. Ed. **46**, 4894 (2007).

[81] S. Wendt, P. T. Sprunger, E. Lira, G. K. H. Madsen, Z. Li, J. Ø. Hansen, J. Matthiesen, A. Blekinge-Rasmussen, E. Lægsgaard, B. Hammer, and F. Besenbacher, Science **320**, 1755 (2008).

[82] A. Tilocca, C. Di Valentin, and A. Selloni, J. Phys. Chem. B **109**, 20963 (2005).

[83] P. A. Redhead, Vacuum **12**, 203 (1962).

[84] In the calculation of the transition path for water dissociation at O vacancies, we have not preadsorbed the water molecules in the defect and then searched for a subsequent dissociation barrier as it was done in Ref. 91, but have started from a water molecule in the gas phase.

[85] K. R. Paserba and A. J. Gellman, Phys. Rev. Lett. **86**, 4338 (2001).

[86] G. S. Herman, Z. Dohnálek, N. Ruzycki, and U. Diebold, J. Phys. Chem. B **107**, 2788 (2003).

[87] A. D. Becke, Phys. Rev. A **38**, 3098 (1988).

[88] J. P. Perdew, Phys. Rev. B **33**, 8822 (1986); **34**, 7406(E) (1986).

[89] J. P. Perdew, J. A. Chevary, S. H. Vosko, K. A. Jackson, M. R. Pederson, D. J. Singh, and C. Fiolhais, Phys. Rev. B **46**, 6671 (1992); **48**, 4978(E) (1993).

[90] B. Hammer, L. B. Hansen, and J. K. Norskov, Phys. Rev. B **59**, 7413 (1999).

[91] S. Kajita, T. Minato, H. S. Kato, M. Kawai, and T. Nakayama, J. Chem. Phys. **127**, 104709 (2007).

[92] F. Allegretti, S. O'Brien, M. Polcik, D. I. Sayago, and D. P. Woodruff, Phys. Rev. Lett. **95**, 226104 (2005).

[93] B. Meyer, D. Marx, O. Dulub, U. Diebold, M. Kunat, D. Langenberg, and Ch. Wöll, Angew. Chem. **116**, 6809 (2004); Angew. Chem., Int. Ed. **43**, 6641 (2004).

[94] O. Dulub, B. Meyer, and U. Diebold, Phys. Rev. Lett. **95**, 136101 (2005).

[95] B. Meyer, H. Rabaa, and D. Marx, Phys. Chem. Chem. Phys. **8**, 1513 (2006).